A Comparative Study to Reveal the Influence of Typhoons on the Transport, Production and Accumulation of O_3 in the Pearl River Delta, China

Kun Qu[1,2], Xuesong Wang[1,2], Yu Yan[1,2], Jin Shen[3], Teng Xiao[1,2], Huabin Dong[1,2], Limin Zeng[1,2], and Yuanhang Zhang[1,2,4,5]

[1]State Key Joint Laboratory of Environmental Simulation and Pollution Control, College of Environmental Sciences and Engineering, Peking University, Beijing 100871, China
[2]International Joint Laboratory for Regional Pollution Control, Ministry of Education, Beijing, 100816, China
[3]State Key Laboratory of Regional Air Quality Monitoring, Guangdong Key Laboratory of Secondary Air Pollution Research, Guangdong Environmental Monitoring Center, Guangzhou 510308, China
[4]Beijing Innovation Center for Engineering Science and Advanced Technology, Peking University, Beijing 100871, China
[5]CAS Center for Excellence in Regional Atmospheric Environment, Chinese Academy of Sciences, Xiamen 361021, China

Correspondence to: Xuesong Wang (xswang@pku.edu.cn) and Yuanhang Zhang (yhzhang@pku.edu.cn)

Abstract. The Pearl River Delta (PRD) region in South China is faced with severe ambient O_3 pollution in autumn and summer, which mostly coincides with the occurrence of typhoons above the Northwest Pacific. With increasingly severe O_3 pollution in the PRD under the influence of typhoons, it is necessary to gain a comprehensive understanding of the impact of typhoons on O_3 transport, production and accumulation for efficient O_3 reduction. In this study, we analysed the general influence of typhoons on O_3 pollution in the PRD via systematic comparisons of meteorological conditions, O_3 processes and sources on O_3 pollution days with and without typhoon occurrence (denoted as the typhoon-induced and no-typhoon scenarios, respectively), and also examined the differences in these influences in autumn and summer. The results show that the approach of typhoons was accompanied by higher wind speeds and strengthened downdrafts in autumn as well as the inflows of more polluted air masses in summer, suggesting favourable O_3 transport conditions in the typhoon-induced scenario in both seasons. However, the effect of typhoons on the production and accumulation of O_3 were distinct. Typhoons led to reduced cloud cover, and thus stronger solar radiation in autumn, which accelerated O_3 production, but the shorter residence time of local air masses was unfavourable for the accumulation of O_3 within the PRD. In contrast, in summer, typhoons increased cloud cover, and weakened solar radiation, thus restraining O_3 formation, but the growing residence time of local air masses favoured O_3 accumulation. The modelling results using the Community Multiscale Air Quality (CMAQ) model for the typical O_3 pollution days suggest increasing contributions from the transport processes as well as sources outside the PRD for O_3 pollution, confirming enhanced O_3 transport under typhoon influence in both seasons. The results of the process analysis in CMAQ suggest that the chemical process contributed more in autumn but less in summer in the PRD. Since O_3 production and accumulation cannot be enhanced at the same time, the proportion of O_3 contributed by emissions within the PRD was likely to decrease in both seasons. The difference in the typhoon influence on O_3 processes in autumn and summer can be attributed to the seasonal variation of the East Asian monsoon. From the "meteorology-process-source" perspective, this study revealed

34 the complex influence of typhoons on O$_3$ pollution in the PRD and their seasonal differences. To alleviate O$_3$ pollution under

35 typhoon influence, emission control is needed on a larger scale, rather than only within the PRD.

1 Introduction

37 Tropospheric ozone (O$_3$) serves as a secondary pollutant in ambient air and is detrimental for human health and crop

38 production (Wang et al., 2017; Liu et al., 2018; Mills et al., 2018). Ambient O$_3$ is produced from its precursors, i.e., nitrogen

39 oxides (NO$_x$ = NO + NO$_2$) and volatile organic compounds (VOCs), through chemical reactions in the presence of sunlight.

40 Due to the relatively long lifetime of O$_3$ (~22 days; Stevenson et al., 2006), it can accumulate locally, or be transported to

41 downwind regions. Under unfavourable meteorological conditions, enhanced transport, production and/or accumulation of

42 O$_3$ can all contribute to the O$_3$ pollution within a region (National Research Council, 1991).

43

44 As the largest city cluster in South China, the Pearl River Delta (PRD) region is faced with frequent ambient O$_3$ pollution,

45 especially in autumn and summer (Li et al., 2014; Wang et al, 2017; Lu et al, 2018). Along with the continuous increasing of

46 O$_3$ levels in recent years (Li et al., 2019), O$_3$ has become the primary contributor to the deterioration of air quality in this

47 region (Feng et al., 2019). The occurrence of O$_3$ pollution in the PRD is predominantly related to the influence of typhoons

48 (or tropical cyclones) above the Northwest Pacific (Gao et al., 2018; Deng et al., 2019; Lin et al., 2019). According to Gao et

49 al. (2018), seven out of the nine most severe O$_3$ episodes (regional-mean maximum 8-h average O$_3$ concentrations > 240

50 μg/m^3) during 2014–2016 coincided with the approach of typhoons. The changes in the track and intensity of typhoons may

51 contribute to the growing trend of O$_3$ levels recently and in future (Lam, 2018; Lam et al., 2018). Therefore, a

52 comprehensive understanding of the influence of typhoons on the transport, production and accumulation of O$_3$ has

53 important implications for efficient and strategic O$_3$ reduction in the PRD.

54

55 Analyses of typhoon-related O$_3$ episodes in the PRD have been extensively reported in previous publications. The effect of

56 typhoons on O$_3$ pollution is closely linked to meteorological conditions that are conducive to the transport, production and/or

57 accumulation of O$_3$. Stagnation caused by typhoons, characterised by low wind speeds, has been reported during many

58 episodes, and it promotes the accumulation of locally formed O$_3$ within the PRD (Wang et al., 1998; So and Wang, 2003;

59 Wang and Kwok, 2003; Huang et al., 2005; Lam et al., 2005; Jiang et al., 2008; Zhang et al., 2014; Chow et al., 2019).

60 Strong north or west winds were observed or simulated during several episodes, suggesting the potentially strengthened

61 transport of pollutants under typhoon influence (Wang et al., 2001; Yang et al., 2012; Wang et al., 2015; Wei et al., 2016).

62 Downdrafts on the outskirts of typhoons may promote downward O$_3$ transport and contribute to near-ground O$_3$ pollution as

63 well (Lam, 2018), but its appearance in the PRD has only been examined in a few studies. Cloudless conditions and strong

64 solar radiation enhance O$_3$ production, which is another important cause of O$_3$ pollution (Wang et al., 1998; Wang and

65 Kwok, 2003; Li et al., 2018; Yue et al., 2018; Chow et al., 2019). In a more direct way, several studies have utilised

66 chemical transport models, along with the Process Analysis (PA) tool and source apportionment (SA) methods, to quantify

67 and compare the contributions of various O_3 processes (e.g., transport and the chemical process) and sources (e.g., local

68 emissions, outside emissions and background) during these episodes. Based on reports by Huang et al. (2005), Lam et al.

69 (2005), Jiang et al. (2008), Wang et al. (2010), Li (2013), Wang et al. (2015), Wei et al. (2016) and Chen et al. (2018),

70 horizontal/vertical transport and chemical production may both be the main contributing process for typhoon-induced O_3

71 pollution in different parts of the PRD. The SA results revealed that emissions within the PRD contributed 40–80% of O_3

72 during typhoon-related O_3 episodes (Li et al., 2012; Li, 2013; Chen et al., 2015), suggesting the potentially important role of

73 O_3 accumulation for O_3 pollution here. However, despite massive episode-based studies, several important questions still

74 remain: Are O_3 transport, production and accumulation within the PRD all enhanced at the same time by typhoons? Do both

75 O_3 pollution seasons (autumn and summer) experience similar impact of typhoons on O_3 pollution? More thorough

76 investigations are needed to answer these questions.

77

78 In this study, we present systematic comparisons between O_3 pollution in the typhoon-induced and no-typhoon scenarios

79 (definitions given in Sect. 2.2) to elucidate the influence of typhoons on O_3 transport, production and accumulation in the PRD

80 and to reveal their seasonal differences. October and July in 2014–2018 were selected as the representative months for autumn

81 and summer, respectively. Multiple datasets, including the ERA-Interim re-analysis, the routine monitoring datasets,

82 trajectories calculated by the Hysplit model and the modelling results of typical O_3 pollution days using the Community

83 Multiscale Air Quality (CMAQ) model, were used in the comparisons. A detailed introduction of these datasets is presented

84 in Sect. 2. The comparisons were conducted from the perspectives of meteorological conditions (Sect. 3), O_3 processes and

85 sources (Sect. 4), and the conclusions about the influence of typhoons on the causes of ambient O_3 pollution in the PRD in the

86 two seasons are illustrated in Sect. 5.

87 **2 Methods**

88 **2.1 Datasets**

89 The detailed information for the datasets utilised in the comparison of meteorological conditions is presented below:

90 •   **Re-analysis datasets**: We mainly used the ERA-Interim re-analysis product in the analyses due to its more available

91   parameters and high spatial coverage (available at https://www.ecmwf.int/en/forecasts/datasets/reanalysis-datasets/era-

92   interim, last accessed: March 2020; Dee et al., 2011; Berrisford et al., 2011). Specifically, meteorological parameters

93   used in the comparisons include the following three categories: (1) near-surface parameters from the analysis fields,

94   including air temperature (at a height of 2 m), relative humidity (RH, at 1000 hPa), horizontal wind speeds (at a height

95   of 10 m; zonal and meridional wind speeds were also involved in the comparisons), and low (for the height at which

96   pressure/surface pressure > 0.8), medium (for the height at which 0.45 < pressure/surface pressure < 0.8), high (for the

97   height at which pressure/surface pressure < 0.45) and total cloud covers; (2) near-surface parameters from the forecast

98   fields, including plenary boundary layer (PBL) height and net surface solar radiation; and (3) upper air parameters at

99   multiple heights, including horizontal and vertical wind speeds, cloud water content and O_3 mixing ratio. The focus of

100 this study is O_3 pollution during the daytime, and therefore, only the parameters at 14:00 local time (LT) were selected

101 for the analyses (except for net surface solar radiation, which was averaged within 8:00–17:00 LT).

102 • **Surface meteorological routine monitoring datasets**: The routine monitoring meteorological data collected at 29

103 national meteorological sites within the PRD (locations shown in Fig. S1a) were also used to explore the

104 meteorological features under the impact of typhoons. The parameters include air temperature, RH, and wind speed and

105 direction (also transformed to zonal and meridional wind speeds in the comparisons) at 14:00 LT.

106 • **Typhoon information**: The times, locations and intensities of typhoons were provided by the Chinese Meteorological

107 Administration Best Track Dataset of tropical cyclones (Ying et al., 2014). The tracks of all typhoons that potentially

108 contributed to O_3 pollution in the PRD during the study period (October and July in 2014–2018) are shown in Fig. S2

109 and S3.

110 • **O_3 concentrations**: Hourly O_3 concentration data, which were originally released by the China National Environmental

111 Monitoring Centre, were downloaded from http://beijingair.sinaapp.com (last accessed: Dec. 2018). Based on the

112 hourly data, we calculated the maximum 1-hr concentrations (MDA1) and maximum 8-hr average concentrations

113 (MDA8) of O_3 in nine municipalities in the PRD (including Guangzhou, Shenzhen, Zhuhai, Foshan, Jiangmen,

114 Zhaoqing, Huizhou, Dongguan and Zhongshan) to identify O_3 pollution days that served as samples in the comparisons.

115 **2.2 Definition and classification of O_3 pollution days**

116 In this study, O_3 pollution days were defined as the days when the MDA1 exceeds 200 μg/m^3 or the MDA8 exceeds 160

117 μg/m^3 for O_3 (both are the Grade-II thresholds of the Chinese National Ambient Air Quality Standard (NAAQS), GB 3095-

118 2012) in any of the nine municipalities in the PRD. According to these criteria, there were 78 and 55 O_3 pollution days

119 (given in Table S1 and S2) during October and July in 2014–2018, respectively. The information about these O_3 pollution

120 days in the two representative months is listed in Table 1 (overall) and S3 (monthly), including the numbers of days, their

121 proportions in the month, and the corresponding mean O_3 concentrations (MDA8 and MDA1, highest values among nine

122 municipalities in the PRD). Although there were more O_3 pollution days in October than in July, O_3 pollution under typhoon

123 influence occurred on ~30% days of both months. Higher O_3 MDA1 and MDA8 values can be found with the appearance of

124 typhoons in comparison with days without typhoons in July, whereas these values are similar in October, indicating the

125 important role of typhoons in O_3 pollution in the PRD.

126

127 The differing locations of typhoons can result in the diverse effect of typhoons on O_3 pollution (Chow et al., 2018). To

128 determine the general influence of typhoons on O_3 pollution in the PRD, it was necessary to further select O_3 pollution days

129 coinciding with typhoons with similar directions and distances to the PRD. As is shown in Fig. 1, all O_3 pollution days in

130 October and most O_3 pollution days in July under typhoon influence were associated with typhoons to the east of the PRD,

131 which were more likely to cause O_3 pollution (Chow et al., 2018). In order to minimize the disturbance of typhoon directions

132 in the comparisons, we removed the remaining five O_3 pollution days in July with typhoons located to the due north or

133 southwest of the PRD from the analyses. After this, based on the distances between typhoon centres and the PRD (at 14:00

134 LT), we classified the pollution days with typhoons in each season into three categories: close typhoon (lowest 20% of

135 distances), typhoon (20–80% intervals of distances), and far typhoon (longest 20% of distances)-induced days. The typhoon-

136 induced days represent O_3 pollution days with general typhoon influence, and they were compared with those without the

137 appearance of typhoons (hereafter denoted as the no-typhoon days). It should be noted that the distances between typhoon

138 centres and the PRD on the typhoon-induced days were overall larger in autumn (1400–2800 km, at 14:00 LT) than in

139 summer (700–2000 km, at 14:00 LT), which may be the consequence of the different characteristics of typhoon paths in the

140 two seasons: most typhoons in autumn travel northwest initially and then turn northward in the areas east of the Philippines

141 (Fig. S2), whereas they are more likely to end up landing in Southeast China in summer (Fig. S3). Since the influence of

142 typhoons on O_3 pollution may be different when typhoons come close enough to the PRD (Lam et al., 2005; Li, 2013), the

143 close typhoon-induced days were considered to be a special scenario in the comparisons of meteorological conditions (Sect.

144 3.5). Owing to the less apparent effect of typhoons over the PRD, we did not include the far typhoon-induced days in the

145 discussions.

146

147 **Table 1.** The numbers and proportions of O_3 pollution days, and O_3 concentrations for various scenarios.

Parameter	October, 2014–2018	July, 2014–2018
Number (proportion) of O_3 pollution days	78 (50.3%)	55 (35.5%)
With typhoons	49 (31.6%)	45 (29.0%)
Typhoon-induced days	30 (19.4%)	24 (15.5%)
Close typhoon-induced days	10 (6.5%)	8 (5.2%)
Without typhoons (no-typhoon days)	29 (18.7%)	10 (6.5%)
Mean PRD-max O_3 MDA8 ($\mu g/m^3$)		
With typhoons	195.0	205.3
Typhoon-induced days	199.5	205.4
Close typhoon-induced days	184.6	225.7
Without typhoons (no-typhoon days)	189.8	187.8
Mean PRD-max O_3 MDA1 ($\mu g/m^3$)		
With typhoons	230.4	259.8
Typhoon-induced days	235.2	260.0
Close typhoon-induced days	219.2	277.1
Without typhoons (no-typhoon days)	231.5	246.5

148

149

150
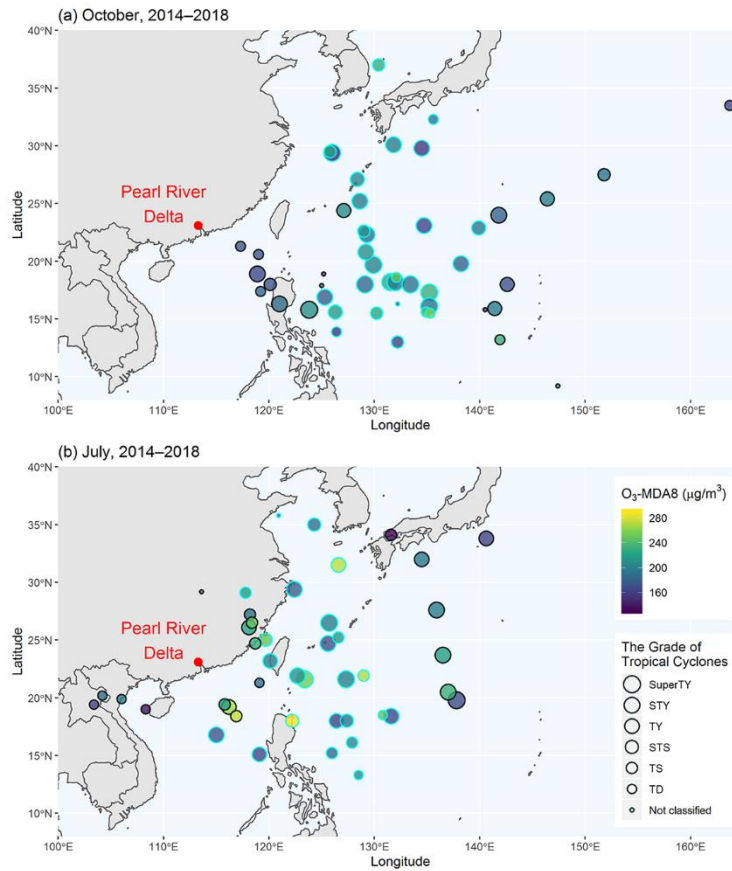
Figure 1. The location and intensity of typhoons at 14:00 LT on all O_3 pollution days with typhoons, and the corresponding O_3 MDA8 concentrations (maximum values in the nine municipalities of the PRD) on the same days during (a) October and (b) July in 2014–2018. The points with cyan borders indicate the "typhoon-induced" O_3 pollution days used in the comparisons. The grades of tropical cyclones (Chinese National Standard, GB/T 19201-2006) are as follows: SuperTY - super typhoon; STY - severe typhoon; TY - typhoon; STS - severe tropical storm; TS - tropical storm; TD - tropical depression; others are grouped as "not classified".

2.3 Calculation of the trajectories and air parcel residence time

To explore the potential effect of cross-regional transport on O_3 pollution in the PRD, we applied the Hysplit model (Stein et al., 2015) with the Global Data Assimilation System (GDAS) datasets as inputs to calculate 72-h backward trajectories reaching the PRD at 14:00 LT for all O_3 pollution days. The Modiesha site (23.1 °N, 113.3 °E; Fig. S1b), which is located in the central part of the PRD, was the endpoint of backward trajectories. Its height was set as 500 m above the ground to better represent the effect of long-range transport on O_3 pollution, as well as to minimize the disturbance of objects near the surface to the transport (Park et al., 2007).

Air parcel residence time (APRT), discussed by Huang et al. (2019), is the average number of hours that air parcels originated from one place stay within a pre-defined domain, and long APRTs can be used to indicate good accumulation conditions for

166 locally sourced pollutants. To calculate APRTs in the PRD, we designed a 21×15 point matrix (resolution: 0.2 °×0.2 °) that

167 embraces the whole PRD (Fig. S4), and forward trajectories starting from these points were also calculated using the Hysplit

168 model. The height of all points was set as 100 m above the ground to represent the height of all local emissions and to reduce

169 the disturbance of the surface, as well. The start times were set as 2:00, 8:00, 14:00 and 20:00 LT for all O_3 pollution days.

170 Afterwards, the length of time each trajectory remained within the administration borders of the PRD, i.e., APRT, was

171 calculated and attributed to its starting point. APRTs in each point were averaged, and these averaged APRT values in all

172 points were interpolated using the Kriging method to obtain field results for the further comparisons.

173 **2.4 CMAQ modelling: basic setups and modelling methods**

174 We utilised the widely used 3D chemical transport model CMAQ (version 5.0.2) to investigate the effects of typhoons on O_3

175 processes and sources. October 2015 and July 2016 featured the most severe O_3 pollution under typhoon influence among all

176 representative months of the two seasons (Table S3), and thus, they were chosen as the period in the modelling (because there

177 was no severe O_3 pollution during the first 10 days of October 2015 and 3–5 November can be classified as the no-typhoon O_3

178 pollution days, we adjusted the modelling period in autumn to 11 October–10 November 2015) and all typhoon-induced and

179 no-typhoon O_3 pollution days in these two months served as representative O_3 pollution days in the comparisons. In detail,

180 there were four typhoon-induced O_3 pollution days (14–16 and 21 October 2015) and four no-typhoon O_3 pollution days (28

181 October and 3–5 November 2015) in October 2015, whereas there were four and six typhoon-induced and no-typhoon days in

182 July 2016, respectively (typhoon-induced: 7–8 and 30–31 July 2016; and no-typhoon: 22–26 and 29 July 2016). The results of

183 daytime (9:00–17:00 LT) O_3 PA and SA on the above O_3 pollution days were averaged for the typhoon-induced and no-

184 typhoon scenarios in autumn (October 2015) and summer (July 2016) and were used in the comparisons.

185

186 The main setups of the CMAQ model are presented as follows. Two-nested modelling domains with the resolutions of 36 and

187 12 km (denoted as d01 and d02, respectively) were set in this study (Fig. 2). Specifically, d02 covers the whole East and

188 Central China (EC-China), enabling us to evaluate the contribution of emissions in these areas to O_3 pollution in the PRD.

189 There were 19 vertical layers in the CMAQ modelling, with about 10 layers within the PBL (about 0–1 km in heights; Guo et

190 al., 2016). The Weather Research and Forecasting (WRF) model (version 3.2) provided the meteorological fields used as inputs.

191 SMOKE (version 2.5) and MEGAN (version 2.10) were used to process the anthropogenic and biogenic emission files,

192 respectively. The anthropogenic emission inventory used in this study consisted of the following three parts: (1) emissions in

193 the PRD, which were provided by the Guangdong Environmental Monitoring Centre; (2) emissions in other areas of mainland

194 China, which were extracted from the MEIC inventory (He, 2012); and (3) emissions in other countries and regions in Asia,

195 which were extracted from the MIX inventory (Li et al., 2017). The initial and boundary conditions of the d01 modelling were

196 obtained from the same-period results of the MOZART-4 global model (available at https://www.acom.ucar.edu/wrf-

197 chem/mozart.shtml, last accessed: Dec. 2019), and those of the d02 modelling were extracted from the d01 modelling results.

198 The SAPRC07 gas-phase chemistry mechanism (Carter, 2010) and the AERO6 aerosol scheme were set in the modelling. In

199 addition, the simulations of the two months were both started 10 days ahead to minimise the disturbance of the bias of the

200 initial conditions. The modelling performances of CMAQ and WRF were determined to be acceptable based on the

201 comparisons between the observational and modelling series of meteorological parameters, O_3 MDA8, daily NO_2

202 concentrations and the mixing ratios of non-methane hydrocarbons (NMHCs) in the PRD (for details, refer to Sect. 1 in the

203 Supplement Information), which ensures the validity of the further analyses.

204
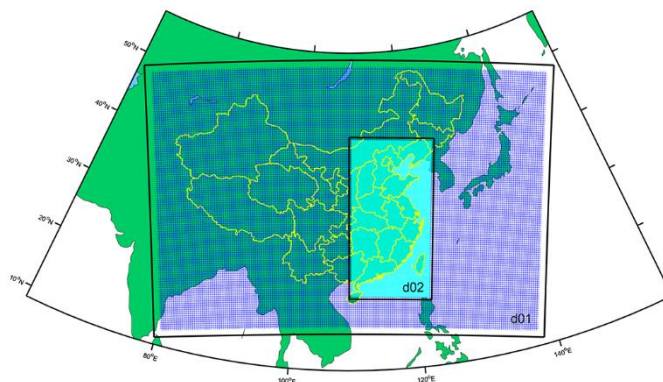
205

206 **Figure 2.** Two-nested modelling domain, noted as d01 and d02. The black boxes indicate the WRF modelling domains, and the nested
207 areas are the CMAQ modelling domains.

208 The PA tool in CMAQ was implemented to quantify the hourly contributions of O_3 processes (or integrated process rate, IPR),

209 which includes vertical/horizontal transport (convection+diffusion), chemical process (net O_3 production through gas-phase

210 reactions), dry deposition and cloud process. To explore the overall effect of typhoons on O_3 transport and production in the

211 region, the mean PA results within the administration boundaries of the PRD were calculated and compared.

212

213 In order to identify the sources of all O_3 in the PRD, we used the classic Brute Force Method (BFM) to identify the contributions

214 of emissions (including anthropogenic and biogenic emissions) in the PRD and other regions in the d02 (mainly EC-China),

215 as well as regions outside the d02 (the boundary conditions of the d02) for O_3 pollution in the PRD (hereafter denoted as the

216 contributions of PRD, EC-China and BCON, or S_{PRD}, $S_{EC\text{-}China}$ and S_{BCON}, respectively). For a pollutant, the contribution of a

217 specific emission, E_i, can be calculated in two ways: (1) the difference between the modelled concentrations of the base case

218 (all emissions involved) and the sensitivity case where E_i is zeroed out (i.e., top-down BFM); (2) the difference between two

219 sensitivity cases where emissions expect E_i and all of the emissions are zeroed out, respectively (i.e., bottom-up BFM). Owing

220 to the non-linearity between O_3 and its precursors, biases may occur between the results of two types of BFM methods, leading

221 to the non-additivity of the results (Clappier et al., 2017). Therefore, the average of the top-down and bottom-up BFM results

222 was treated as the quantified contributions of the concerned sources. Four simulation cases were run in this study, including

223 (the modelled O_3 concentration in each case was also marked in brackets):

224 • the base case (C_{base});

225 • the PRD-cut case (C_{PRD_cut}), where emissions within the PRD were zeroed out;

226 • the PRD-only case (C_{PRD_only}), where emissions outside the PRD (within d02) were zeroed out; and

227 • the zero-emission case (C_0), where all emissions within the d02 were zeroed out.

228 Afterwards, the S_{PRD}, $S_{EC\text{-}China}$ and S_{BCON} values (in concentrations) in the polluted areas of the PRD (where modelled daytime

229 O_3 concentrations > 160 μg/m³, the Grade-II O_3 MDA8 thresholds of the Chinese NAAQS) were calculated using the following

230 equations,

$$S_{PRD} = \frac{1}{2}\left[\left(C_{base} - C_{PRD\_cut}\right) + \left(C_{PRD\_only} - C_0\right)\right], \tag{R1}$$

$$S_{EC-China} = \frac{1}{2}\left[\left(C_{base} - C_{PRD\_only}\right) + \left(C_{PRD\_cut} - C_0\right)\right], \tag{R2}$$

$$S_{BCON} = C_0. \tag{R3}$$

231 The percentage forms of these values were used in the comparisons.

232 **3 Comparison of meteorological conditions**

233 **3.1 Overview: comparison of meteorological parameters in the PRD**

234 First, we compared near-ground meteorological parameters in the PRD on the typhoon-induced and no-typhoon O_3 pollution

235 days. The parameters from routine monitoring datasets (including air temperature, RH, wind speed, zonal and meridional

236 wind speeds measured at 14:00 LT of all O_3 pollution days at 29 national meteorological sites within the PRD (Fig. S1a))

237 and the ERA-Interim re-analysis (including all near-surface parameters from the analysis and forecast fields introduced in

238 Sect. 2.1, extracted at the same time and the locations of sites as these in routine monitoring datasets) were used in the

239 comparison (since all O_3 pollution days in October and over 60% of O_3 pollution days in July were characterized with sunny,

240 cloudy, or overcast weathers with no rainfall in the PRD (Table S4, represented by the weather in Guangzhou), precipitation

241 was not considered in the comparisons). The Mann-Whitney U test was applied to determine whether the above parameters

242 were significantly different ($p < 0.05$) between typhoon-induced and no-typhoon O_3 pollution days.

243

244 As is listed in Table 2, statistically significant differences between the typhoon-induced and no-typhoon scenarios existed for

245 most of the parameters, such as meridional (south-north) wind speed, cloud covers within various height ranges and net

246 surface solar radiation — in both seasons, these parameters were significantly different for the two scenarios. It indicates that

247 the causes of O_3 pollution may vary on typhoon-induced and no-typhoon O_3 pollution days. Note that air temperature, one of

248 the parameters most closely related to O_3 pollution in the PRD (Zhao et al., 2019), was not significantly different in the two

249 scenarios. We also found that the comparison in autumn and summer did not produce the same results: the typhoon-induced

250 days in autumn featured lower RH, stronger winds (especially north wind), reduced cloud cover (low, medium, high and

251 total) and stronger surface solar radiation, whereas in summer, these days had higher RH, weaker south winds, more cloud

252 cover (medium, high and total), weaker surface solar radiation and lower PBL heights. Therefore, the impact of typhoons on

253 O₃ pollution differs in the two seasons, as well. In order to reveal the impact of typhoons on O_3 transport, production, and

254 accumulation in the PRD, more detailed comparisons of the corresponding meteorological indicators are presented in the

255 following sections.

256

257 **Table 2.** The comparisons of meteorological parameters (all at 14:00 LT except for net surface solar radiation, which is the average value
258 for 9:00–17:00 LT) in the PRD for the three scenarios (no-typhoon, typhoon-induced, close typhoon-induced) in two seasons (autumn,
259 summer). RM, routine measurement; ERA, ERA-Interim re-analysis. All of the parameters are presented as "the mean value ± standard
260 deviation". The differences between parameters in the typhoon-induced or close typhoon-induced scenarios and the corresponding
261 typhoon-induced scenarios for the same season are given in parentheses, and "*" indicates $p < 0.05$, or statistically significant differences
262 between these parameters when the Mann-Whitney U test is used.

Parameters	Data Source	Autumn (October, 2014–2018)			Summer (July, 2014–2018)		
		No-typhoon	Typhoon-induced	Close Typhoon-induced	No-typhoon	Typhoon-induced	Close Typhoon-induced
Air Temperature (℃)	RM	29.1 ±2.2	29.3 ±1.8 (+0.2)	29.6 ±1.5 (+0.5, *)	33.7 ±2.0	33.9 ±2.0 (+0.2)	35.0 ±1.5 (+1.3, *)
	ERA	29.2 ±2.1	29.3 ±1.6 (+0.1)	29.6 ±1.5 (+0.4, *)	33.4 ±1.8	33.5 ±1.4 (+0.1)	34.6 ±1.4 (+1.2, *)
RH (%)	RM	52.4 ±10.2	44.8 ±10.4 (-7.6, *)	51.4 ±12.4 (-1.0)	57.0 ±9.3	58.3 ±9.7 (+1.3)	56.9 ±6.4 (-0.1)
	ERA	54.0 ±9.8	48.3 ±11.2 (-5.7, *)	52.2 ±12.4 (-1.8, *)	62.6 ±10.8	66.4 ±9.4 (+3.8, *)	62.5 ±9.4 (+0.1)
Wind Speed (m/s)	RM	2.33 ±1.18	2.58 ±1.23 (+0.25, *)	2.96 ±1.40 (+0.63, *)	2.46 ±1.33	2.30 ±1.20 (-0.16)	2.53 ±1.16 (+0.07)
	ERA	2.39 ±1.30	2.54 ±0.99 (+0.15, *)	3.53 ±1.11 (+1.14, *)	2.41 ±0.99	2.18 ±1.18 (-0.23, *)	2.61 ±1.05 (+0.20)
Zonal (East-West) Wind Speed (m/s)	RM	-0.83 ±1.72	-0.59 ±1.70 (+0.24, *)	-0.13 ±1.74 (+0.70, *)	-0.41 ±2.05	-0.03 ±1.94 (+0.38)	0.73 ±1.98 (+1.14, *)
	ERA	-1.41 ±1.43	-1.07 ±1.04 (+0.34, *)	-0.87 ±0.79 (+0.54, *)	0.22 ±1.73	-0.02 ±1.81 (-0.24)	0.29 ±2.45 (+0.07)
Meridional (South-North) Wind Speed (m/s)	RM	-0.36 ±1.74	-1.49 ±1.66 (-1.13, *)	-2.21 ±1.66 (-1.85, *)	0.79 ±1.69	0.01 ±1.72 (-0.78, *)	-0.69 ±1.68 (-1.48, *)
	ERA	-0.27 ±1.82	-1.97 ±1.16 (-1.70, *)	-3.27 ±1.29 (-3.00, *)	1.61 ±1.09	0.64 ±1.58 (-0.97, *)	-0.68 ±1.19 (-2.29, *)
Low Cloud Cover (%)	ERA	17.2 ±22.7	4.2 ±11.9 (-13.0, *)	15.5 ±23.9 (-1.7, *)	8.7 ±9.4	7.1 ±9.5 (-1.6, *)	5.2 ±5.0 (-3.5, *)
Medium Cloud Cover (%)	ERA	22.2 ±26.5	10.4 ±19.7 (-11.8, *)	9.5 ±14.5 (-12.7, *)	8.7 ±11.1	15.4 ±15.1 (+6.7, *)	21.5 ±15.5 (+12.8, *)
High Cloud Cover (%)	ERA	12.1 ±23.1	7.2 ±16.3 (-4.9, *)	34.6 ±35.6 (+22.5, *)	32.2 ±30.0	44.9 ±29.3 (+12.7, *)	51.0 ±34.2 (+18.8, *)
Total Cloud Cover (%)	ERA	43.5 ±32.3	20.5 ±25.7 (-23.0, *)	51.9 ±33.1 (+8.4, *)	43.7 ±26.7	58.3 ±22.7 (+14.6, *)	67.5 ±21.0 (+23.7, *)
Net Surface Solar Radiation (W/m²)	ERA	456.9 ±78.4	516.6 ±66.7 (+59.7, *)	516.5 ±62.8 (+59.6, *)	560.3 ±93.1	523.2 ±74.4 (-37.1, *)	541.9 ±54.0 (-18.4, *)
PBL Height (m)	ERA	1471 ±315	1473 ±348 (+2)	1349 ±227 (-122, *)	1268 ±383	1037 ±289 (-231, *)	1196 ±300 (-72, *)

3.2 O$_3$ transport conditions: comparison of wind speeds, backward trajectories and vertical air motions

The higher wind speeds and/or O$_3$ levels in the transported air masses are, the more likely O$_3$ transport plays an increasingly important role in O$_3$ pollution. In the PRD, O$_3$ levels are closely linked to the type of air masses influencing the region, which can be identified based on backward trajectories. According to Zheng et al. (2010), there are generally three types of air masses that are transported into the PRD along different paths and contribute to O$_3$ pollution here, namely, the continental, coastal and marine air masses (Fig. 3a). The continental and coastal air masses can bring O$_3$ from EC-China to the PRD, and thus, they are typically recognised as being polluted and contributing to relatively high O$_3$ levels in the PRD. In contrast, the marine air masses, originated from the South China Sea, are much cleaner. In this section, we studied the influence of typhoons on O$_3$ transport by comparing wind speeds and 72-h backward trajectories in the typhoon-induced and no-typhoon scenarios.
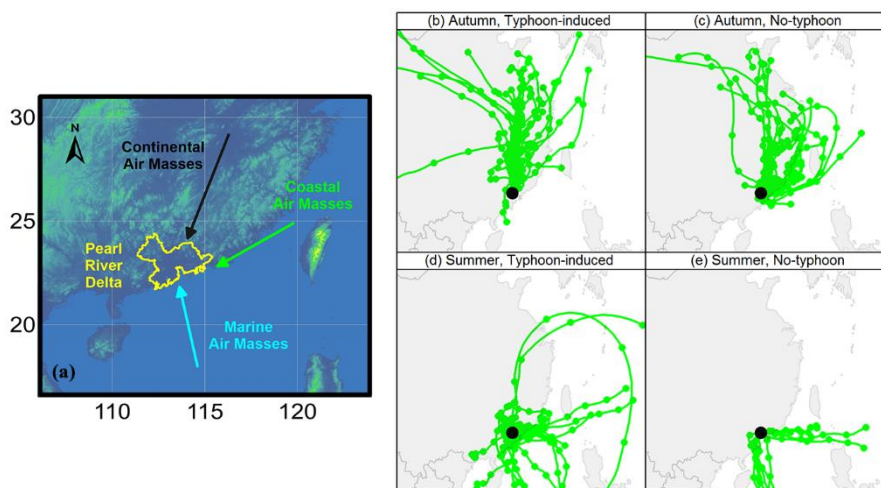
Figure 3. (a) Three O$_3$ transport paths towards the PRD. (b–e) Backward trajectories at 14:00 LT for each scenario: (b) autumn, typhoon-induced; (c) autumn, no-typhoon; (d) summer, typhoon-induced; and (e) summer, no-typhoon. The black dots indicate the end point of all trajectories, i.e., where the Modiesha site in the central PRD is located.

As is displayed in Fig. 3b–c, we identified the influence of continental air masses on the typhoon-induced O$_3$ pollution days in autumn, as well as mixed contributions from the continental and coastal air masses on the corresponding no-typhoon days. However, for the former scenario, significantly increased wind speeds (Table 2) ensure more favourable conditions for the transport of O$_3$. In summer, the three types of air masses may all have affected O$_3$ pollution in the typhoon-induced scenario, while only the marine air masses influenced the PRD in the no-typhoon scenario (Fig. 3d–e). The increasing influence of much more polluted air masses (continental and coastal air masses) led by typhoon ensured that more O$_3$ was transported to the PRD, thus typhoons also tended to increase the contribution of transport to O$_3$ pollution in the PRD in summer. In addition, the influence of different air masses was also accompanied with variations in the prevailing winds in the PRD, that is, north winds and easterlies in the typhoon-induced and no-typhoon scenarios in autumn, respectively, and southwest winds in the no-typhoon scenario in summer (indicated by wind roses in Fig. S5). For the typhoon-induced scenario in summer, the dominate

287   wind direction is hard to determine. These variations in the local wind fields potentially result in the different spatial
288   distribution of O_3 concentrations in various scenarios.

289

290   Downdrafts are typically considered to be an important cause of typhoon-induced O_3 pollution (Lam, 2018), but in which
291   scenarios downdrafts influence the PRD remains unclear. Thus, we explored the overall features of vertical air motions from
292   the surface layer to the tropopause in the typhoon-induced and no-typhoon scenarios, and the ERA-Interim reanalysis dataset
293   (including all upper air parameters at multiple heights introduced in Sect. 2.1) was utilised in the comparisons. The contours
294   in Fig. 4 show the cross sections of mean vertical wind speed at 14:00 LT of all O_3 pollution days corresponding to the typhoon-
295   induced and no-typhoon scenarios of two seasons, which were made along the 113.2 °E longitude line, from 26.0 °N to 20.0 °N
296   (Fig. S4). On the typhoon-induced days in autumn, downdrafts occurred over large areas above the PRD, especially above a
297   height of ~700 hPa. Although updrafts can still be found near the sea surface in this scenario, vertical wind speeds tended to
298   be lower compared with those on the no-typhoon days in autumn, which also suggests the enhancement of downdrafts caused
299   by typhoons. In summer, the influence of downdrafts was found over the PRD under 850 hPa on the typhoon-induced O_3
300   pollution days. However, overall, updrafts prevailed above the land areas and downdrafts prevailed above the sea in both the
301   typhoon-induced and no-typhoon scenarios in summer, which is recognised as the structure of the East Asian summer monsoon
302   cell (Chen et al., 1964; Jin et al., 2013; Ding et al., 2018). For both updrafts and downdrafts, the absolute values of vertical
303   wind speeds in the typhoon-induced scenario in summer were overall higher than these in the corresponding no-typhoon
304   scenario. Therefore, the approach of typhoons did not break the structure of the summer monsoon cell, but rather they further
305   strengthened the vertical motions above both land areas and sea. These analyses suggest that typhoons do not necessarily lead
306   to downdrafts during O_3 pollution periods in the PRD and its adjacent areas; and in summer, vertical air motions affected by
307   typhoons are more complicated than expected owing to the existence of the East Asian summer monsoon.

308

309   We also explored the regions where downdrafts and updrafts occurred on a larger scale and their potential connections with
310   O_3 levels. As is shown in Fig. 5, though updrafts appeared in the PRD at 850 hPa on the typhoon-induced days in autumn,
311   downdrafts dominated in the region at 700 and 500 hPa. For the areas to the north of the PRD, the important role of downdrafts
312   was found at all three heights. In contrast to the no-typhoon days in autumn, downdrafts tended to cover much larger areas in
313   this scenario. Moreover, these areas at 850 and 700 hPa generally featured higher O_3 mixing ratios as well as lower RH (Fig.
314   S6) than others, which is a sign of possible direct downward O_3 transport (Roux et al., 2020; Wang et al., 2020). This part of
315   O_3 can notably aggravate near-ground O_3 pollution in the PRD. In contrast, in summer, updrafts dominated the PRD at various
316   heights in both scenarios. Besides the PRD, most of the regions near the coast were characterised by updrafts above the land
317   as well as downdrafts offshore, further indicating the ubiquity of the summer monsoon cell. By comparing the two scenarios
318   in summer, we found that typhoons resulted in more areas being influenced by updrafts. The areas with high O_3 levels did not
319   coincide with the downdraft-affected areas, and therefore, O_3 transported from the upper air may play a less significant role in
320   the typhoon-induced O_3 pollution in summer.

321
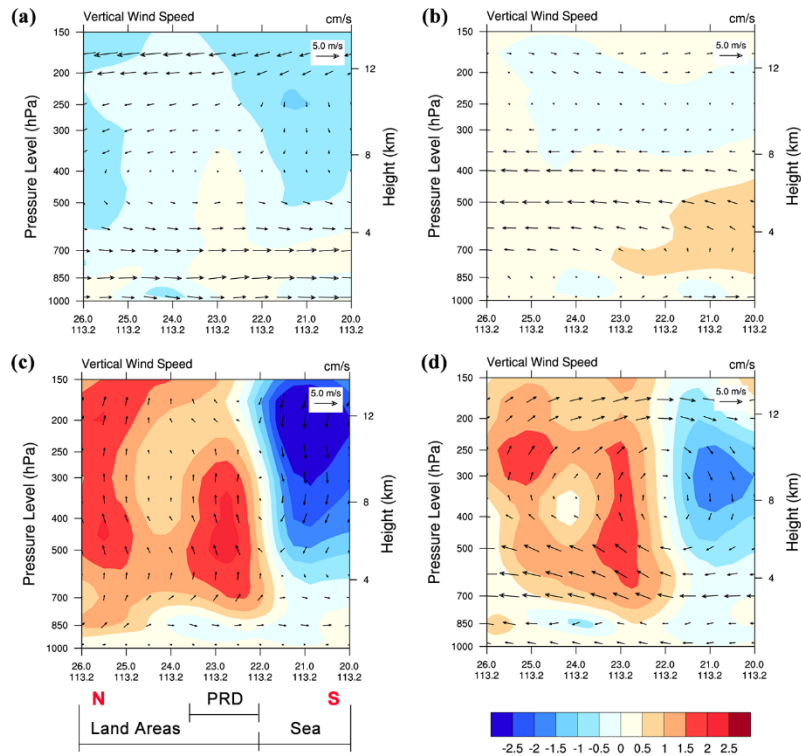
Figure 4. The cross sections of mean vertical wind field at 14:00 LT for each scenario: (a) autumn, typhoon-induced; (b) autumn, no-typhoon; (c) summer, typhoon-induced; and (d) summer, no-typhoon. Cross sections were made along the 113.2 °E longitude line, from 26.0 °N to 20.0 °N (Fig. S4). The vectors indicate meridional wind speed (m/s) and vertical wind speed (cm/s), and the contours indicate vertical wind speed (cm/s). PRD, the Pearl River Delta.

3.3 O₃ production conditions: comparison of clouds

Clouds efficiently reflect solar radiation (Liou, 1976), and therefore, they have a notable impact on the local formation of O_3. Figure 6 displays the cross sections of mean ERA-Interim cloud liquid water contents (CLWC) at 14:00 LT of all O_3 pollution days corresponding to the typhoon-induced and no-typhoon scenarios of two seasons, which were also made along the 113.2 °E longitude line, from 26.0 °N to 20.0 °N (Fig. S4). The comparison of CLWC in the cross sections suggests that typhoons generally resulted in fewer clouds in autumn but more clouds in summer, which agrees well with the comparison of cloud covers in Table 2. The presence of fewer clouds on the typhoon-induced days in autumn can be attributed to two reasons: the influence of dry air masses (indicated by lower RH in Table 2 and Fig. S6) and/or the hindrance of cloud formation by downdrafts. In summer, the strengthened updrafts above the land caused by typhoons favoured cloud formation, which is demonstrated by higher CLWC at the heights of 500–850 hPa and increases in medium and high cloud covers. In areas above the PRD below 850 hPa, downdrafts led to slight decrease of clouds in the typhoon-induced scenario in summer, which is also indicated by reduced low cloud cover. As a consequence of varied cloud covers in each scenario, on average, net surface solar
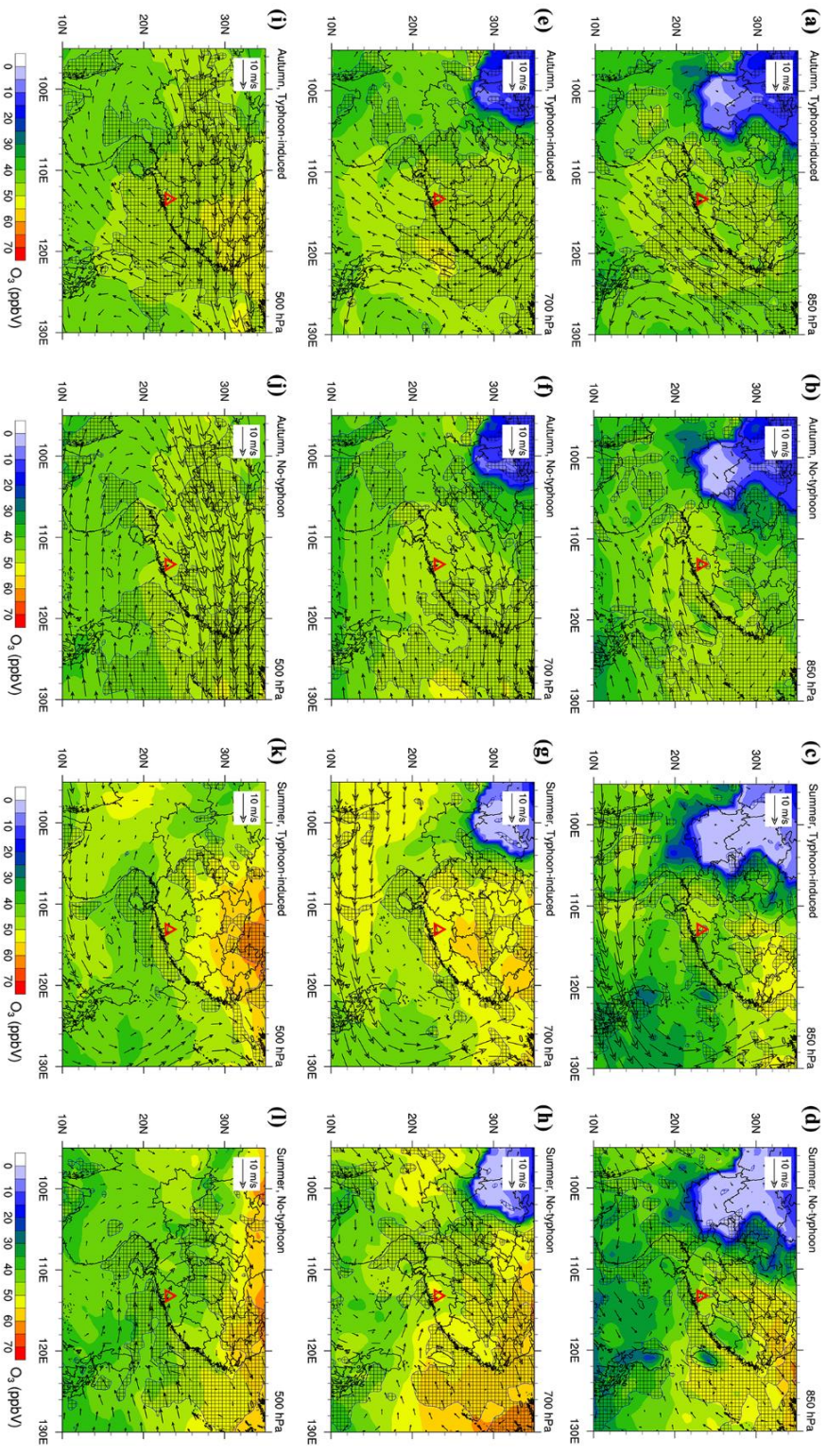
Figure 5. O₃ mixing ratio (ppbV) and wind fields at the height of (a–d) 850 hPa, (e–h) 700 hPa, and (i–l) 500 hPa at 14:00 LT for each scenario: (a, e, i) autumn, typhoon-induced; (b, f, j) autumn, no-typhoon; (c, g, k) summer, typhoon-induced; and (d, h, l) summer, no-typhoon. The red triangle in each plot indicates the PRD. The gridded areas indicate that vertical wind speed is less than 0, or downdrafts occur.

342
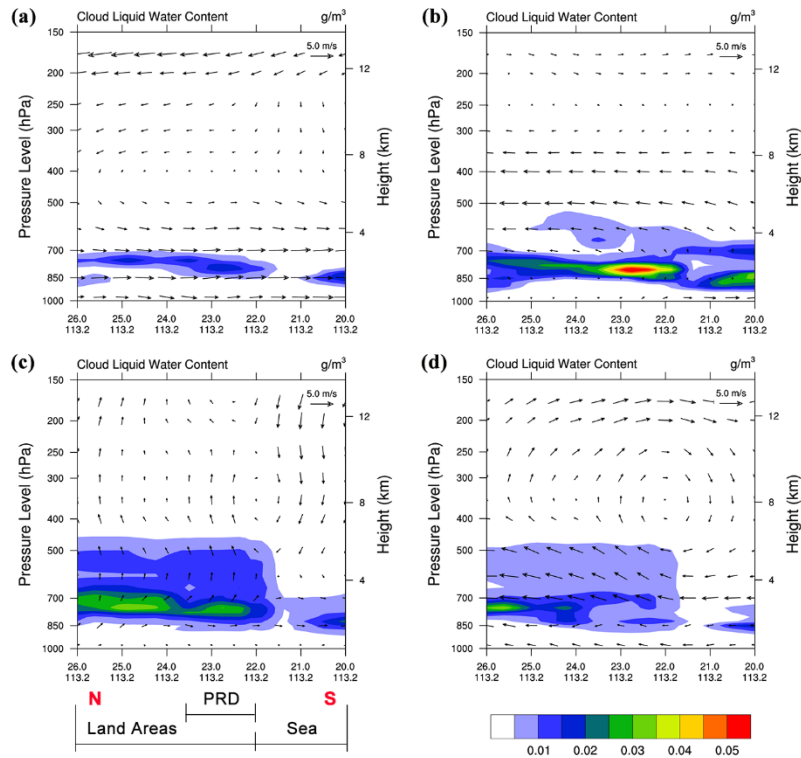
Figure 6. The cross sections of mean cloud liquid water content (g/m³) and wind vectors at 14:00 LT for each scenario: (a) autumn, typhoon-induced; (b) autumn, no-typhoon; (c) summer, typhoon-induced; and (d) summer, no-typhoon. Cross sections were made along the 113.2 °E longitude line, from 26.0 °N to 20.0 °N (Fig. S4). The vectors indicate meridional wind speed (m/s) and vertical wind speed (cm/s). PRD, the Pearl River Delta.

radiation increased by 13% and decreased by 7% on the typhoon-induced days in autumn and summer, respectively (Table 2), which promoted and hindered O_3 production in the PRD during these two seasons, respectively.

3.4 O_3 accumulation conditions: comparison of APRTs

The longer APRTs are, the more likely that O_3 produced by local emissions accumulates within the targeted region and notably contributes to near-ground O_3 pollution. In order to study the effect of typhoons on O_3 accumulation, we calculated APRTs in the PRD in the typhoon-induced and no-typhoon scenarios (Fig. 7) for the further comparisons. On the typhoon-induced days in autumn, APRTs were typically 5–10 hours (mean = 9.5 hours) — shorter than those on the no-typhoon days in autumn (mean = 13.1 hours). In addition, lower APRT values occurred in the central part of the PRD, where high anthropogenic emissions of pollutants are distributed (Zheng et al., 2009). Despite more active O_3 chemistry discussed in the last section, locally sourced O_3 was less likely to accumulate within the PRD in this scenario, potentially limiting the contribution of local emissions for O_3. The comparison suggests opposite results in the summer scenarios, that is, APRTs on the typhoon-induced days (20–30 hours, mean = 21.0 hours) were overall higher than those on the no-typhoon days (15–25 hours, mean = 16.5 hours). This favoured the accumulation of locally sourced O_3, and, to some extent, offset the influence of weakened O_3

360   formation to maintain high contributions of local emissions to O_3 pollution. Based on the comparison of O_3 production

361   conditions in the previous section and the comparison of O_3 accumulation conditions in this section, typhoons did not provide

362   more favourable conditions for O_3 production and accumulation simultaneously in the PRD in both autumn and summer, thus

363   potentially resulting in a less important role of local contributions in O_3 pollution here. More quantitative evaluations of the

364   contributions from multiple O_3 sources are discussed in Sect. 4.

365
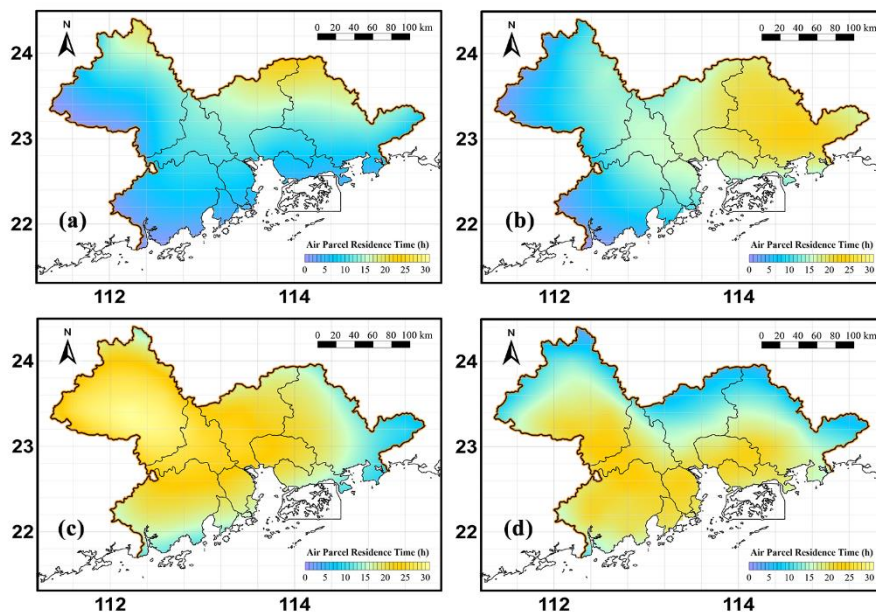
367 **Figure 7.** The spatial distributions of APRTs in the PRD for each scenario: (a) autumn, typhoon-induced; (b) autumn, no-typhoon; (c)
368 summer, typhoon-induced; and (d) summer, no-typhoon.

369 **3.5 Meteorological conditions on the close typhoon-induced days**

370   On the close typhoon-induced days in the two seasons, stronger north winds prevailed and total cloud cover was higher than

371   that on the no-typhoon days (Table 2), suggesting better conditions for the transport of O_3 but less favourable conditions for

372   O_3 production. As displayed in Fig. S7, the APRT values were significantly lower on the close typhoon-induced days (mean

373   = 6.6 hours, 12.9 hours in autumn and summer, respectively) than on the no-typhoon days, making it even harder for locally

374   sourced O_3 to accumulate within the PRD. Therefore, close typhoons are concluded to promote the transport of O_3 from the

375   outside and to reduce the contributions of O_3 produced from local emissions in a more notable way. In addition, close typhoons

376   led to stronger downdrafts in autumn and updrafts in summer than other scenarios in the same season (Fig. S8). It should be

377   noted that the structure of the summer monsoon cell near the PRD was destroyed in the close typhoon-induced scenario in

378   summer, indicating the stronger influence of typhoons on regional wind fields. The dominant role of O_3 transport during O_3

379   pollution days in this special scenario agrees well with the reported episode-based analyses (Lam et al., 2005; Li, 2013).

4 Comparisons of O₃ processes and sources

The comparisons of meteorological conditions served as qualitative evidence to determine the general influence of typhoons on O₃ transport, production and accumulation in autumn and summer. Based on the comparison between the CMAQ modelling results on typical O₃ pollution days in October 2015 and July 2016, more quantitative evidence can be presented. Figure 8 displays modelled mean O₃ MDA8 concentrations and wind fields (at 14:00 LT) on the typhoon-induced and no-typhoon O₃ pollution days of two seasons. Large standard-exceedance (> 160 μg/m³) areas were distributed in the PRD on most days, and the typhoon-induced days of both seasons generally featured higher O₃ levels. The distinct wind fields for these scenarios, which were consistent with those in the longer timespan (Fig. S5), indeed led to different spatial distributions of O₃. Generally, the most severe O₃ pollution occurred in the downwind areas, such as the central and southern parts of the PRD on the typhoon-induced days in October 2015, the central PRD on the no-typhoon days in October 2015, and the northern and eastern PRD on the no-typhoon days in July 2016. On the typhoon-induced days in July 2016, high levels of O₃ accumulated around the PRE. In this section, we discuss the different contributions of various O₃ processes and sources on these days to better understand the effect of typhoons on O₃ pollution in the PRD.
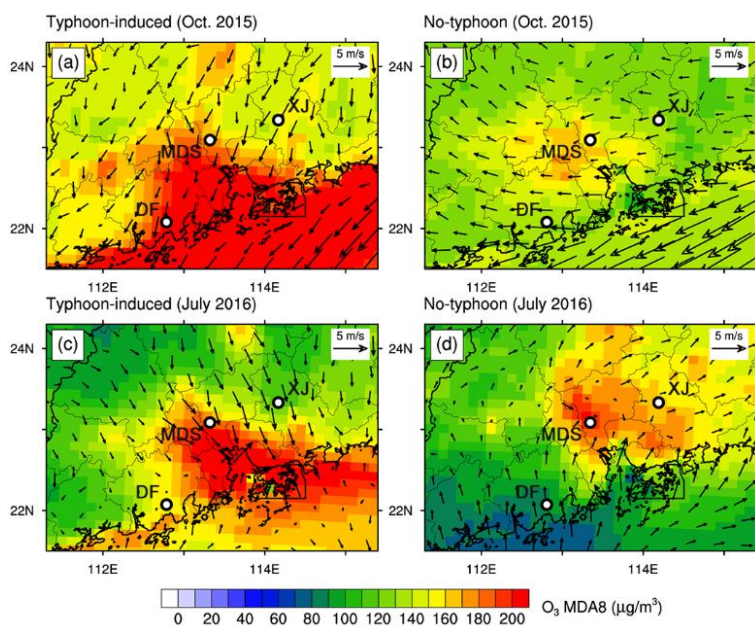
Figure 8. Modelling mean O₃ MDA8 concentrations (μg/m³) and wind vectors (at 14:00 LT) on the representative O₃ pollution days: (a) the typhoon-induced days in October 2015 (14–16 and 21 October 2015); (b) the no-typhoon days in October 2015 (28 October and 3–5 November 2015); (c) the typhoon-induced days in July 2016 (7–8 and 30–31 July 2016); and (d) the no-typhoon days in July 2016 (22–26 and 29 July 2016). Three representative sites in the PRD are shown as black circles in the plots: XJ, Xijiao; MDS, Modiesha; DF, Duanfen.

4.1 O₃ processes: transport vs chemical process

The PA tool in CMAQ was used to quantify the contributions of transport and chemical process to the O_3 variations on O_3 pollution days in October 2015 and July 2016. As is shown in Fig. 9, the daytime (9:00–17:00 LT) O_3 PA results within the PRD in all scenarios share similar characteristics. Dry deposition dominated O_3 removal near the surface, and it also led to high gradients of O_3 concentrations that promote downward O_3 diffusion. Within the PBL (about 0–1 km in height), O_3 was mainly contributed by horizontal transport and chemical process, and vertical convection led to the drop of O_3 concentrations. However, differences existed between the O_3 PA results in the typhoon-induced and no-typhoon scenarios, indicating the impact of typhoons on the transport and production of O_3. In both months, typhoons led to notably higher contribution of horizontal transport to O_3, especially in the lower and middle part of the PBL. Within the PBL, on average, it increased from -0.9 ppb/h, -0.8 ppb/h to 1.2 ppb/h, 2.0 ppb/h under typhoon influence in autumn and summer, respectively. The comparison of the contribution of chemical process (in absolute rates) suggests that they had opposite effects in the two months — under typhoons, the contribution increased in October 2015 (from 4.0 ppb/h to 4.5 ppb/h within the PBL, or by 11.4%), but it decreased in July 2016 (from 7.1 ppb/h to 5.7 ppb/h within the PBL, or by -20.8%). In other words, typhoons promoted and hindered O_3 production in autumn and summer, respectively. These results agree well with the comparisons of O_3 transport and production conditions in the previous section.
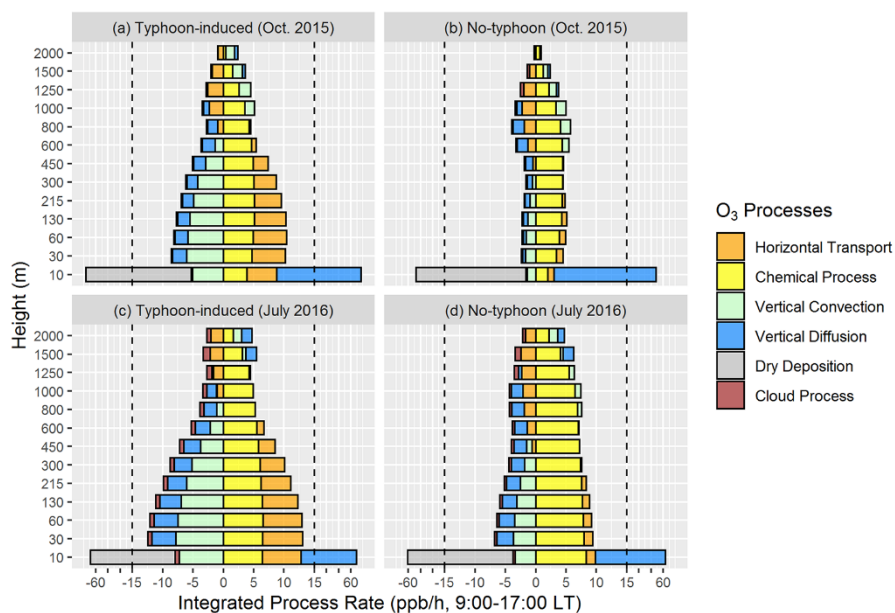
Figure 9. The daytime-mean (9:00–17:00 LT) hourly contributions of O_3 processes within the PRD in vertical layers 1–13 on representative O_3 pollution days: (a) the typhoon-induced days in October 2015 (14–16 and 21 October 2015); (b) the no-typhoon days in October 2015 (28 October and 3–5 November 2015); (c) the typhoon-induced days in July 2016 (7–8 and 30–31 July 2016); and (d) the no-typhoon days in July 2016 (22–26 and 29 July 2016).

4.2 O₃ sources: local sources vs regional sources

The contributions of various sources to O₃ within the PRD are determined by the combined impact of O₃ transport, production and accumulation. The results for mean daytime (9:00–17:00 LT) O₃ SA near the ground (about 0–80 m in height) on typhoon-induced and no-typhoon O₃ pollution days are illustrated in Fig. 10. For polluted regions within the PRD, stronger O₃ production under typhoons did not lead to a higher proportion of local contributions to O₃ pollution in October 2015 — it even decreased from 22% (on the no-typhoon days) to 17% (on the typhoon-induced days). The contributions of EC-China emissions and BCON, in contrast, increased slightly from 37%, 41% to 40%, 43%, respectively. The distinction of the O₃ SA results is more apparent for the summer scenarios, that is, typhoons resulted in growing contributions from O₃ transported from other regions (from 40% to 59%) but decreased local contributions (from 60% to 41%) in July 2016. More favourable O₃ accumulation conditions (indicated by higher APRTs on the representative typhoon-induced O₃ pollution days in summer (Fig. S9)) were far from sufficient to compensate for the effect of weakened O₃ production on the high contributions of local sources.
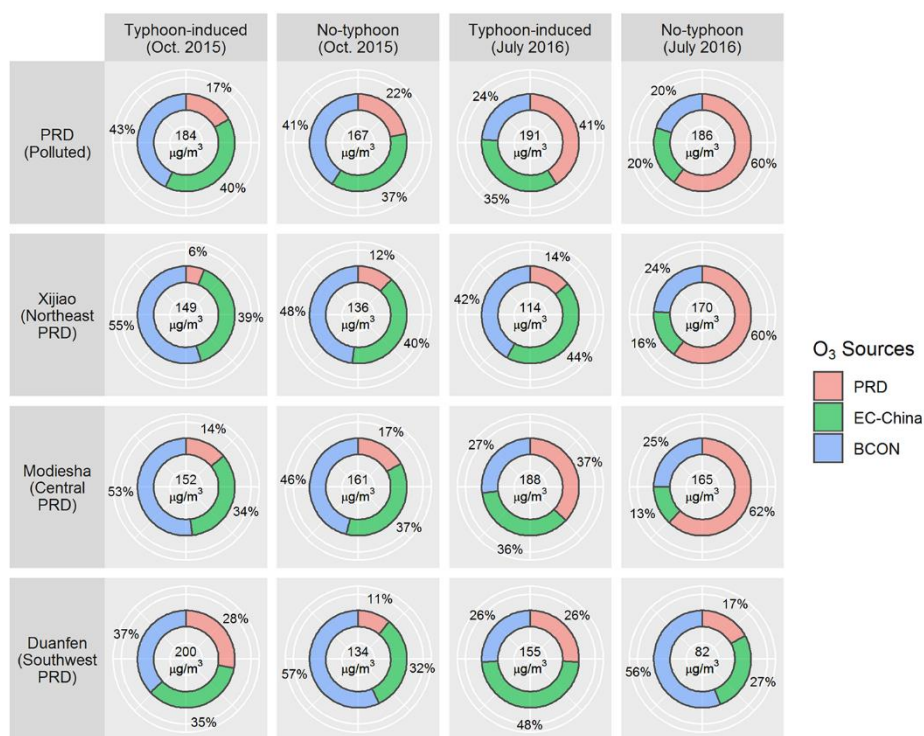
Figure 10. The mean O₃ SA near the ground (about 0–80 m in height) on the represented typhoon-induced and no-typhoon O₃ pollution days in October 2015 and July 2016 (the average results of 9:00–17:00 LT). The locations of the three representative sites (Xijiao, Modiesha and Duanfen) are shown in Fig. 8. PRD, the Pearl River Delta; EC-China, East China and Central China; BCON, the boundary conditions of the d02 modelling.

Furthermore, owing to the variations of wind fields, the comparison results of O₃ SA in different parts of the PRD may differ from the regional ones. For instance, while the comparisons of O₃ SA in the Xijiao and Modiesha site (located in the northeast

440 and central part of the PRD, respectively) agree well with those in the polluted regions of the PRD, higher contributions of

441 PRD emissions for O_3 can be found in the Duanfen site (located in the southwest part of the PRD) on the typhoon-induced

442 days of two months in comparison to these on the corresponding no-typhoon days (Fig. 10). Since the site was located in the

443 downwind region in the typhoon-induced scenario in October 2015 (Fig. 8a), enhanced O_3 production led by typhoons from

444 the massive emissions of O_3 precursors in the central PRD (Zheng et al., 2009) contributed to higher local contributions for O_3

445 pollution here (as the distribution of local contributions in percentage to daytime O_3 shown in Fig. S10, the highest local

446 contribution in the PRD occurred in areas near the Duanfen site and almost reached 40% in this scenario, which was even

447 higher than that in the corresponding no-typhoon scenario (33%)). In the no-typhoon scenario in July 2016, the site was located

448 in the upwind regions under the prevailing of southwest winds, limiting the contributions of local emissions for O_3 at the site

449 (Fig. 8d). Thus, higher local contributions can also be found in the typhoon-induced scenario in this month.

450 **5 Discussion and conclusions**

451 The significance of typhoons on O_3 pollution in the PRD calls for thorough evaluations of the different causes of O_3 pollution

452 with the appearance of typhoons in the Northwest Pacific. In this study, we revealed the different impacts of typhoons on O_3

453 transport, production and accumulation in the PRD (as summarised in Fig. 11) through systematic comparisons of

454 meteorological conditions, the contributions of various O_3 processes and sources in the typhoon-induced and no-typhoon

455 scenarios. We found that typhoons tended to promote O_3 transport towards the PRD, but failed to provide more favourable O_3

456 production and accumulation conditions simultaneously, which limited the contribution of local emissions to O_3 pollution.

457 Furthermore, there were also differences between the influence of typhoons on O_3 pollution in autumn and summer. More

458 favourable transport conditions occurred in the typhoon-induced scenario in autumn, which was characterised by higher wind

459 speeds and the increased influence of downdrafts. In summer, the mixed types of air masses in the typhoon-induced scenario

460 were likely to bring more O_3 into the PRD than the clean marine air masses in the no-typhoon scenario, also suggesting

461 enhanced O_3 transport under the influence of typhoons. Generally, typhoons led to cloudless conditions, stronger solar radiation,

462 and thus more rapid O_3 production in autumn, but shorter APRTs (5–10 hours) suggest that locally sourced O_3 was hard to

463 accumulate within the PRD. As a result, the contributions in percentage of local emissions to O_3 pollution decreased (slightly

464 by ~5% for the polluted regions of the PRD in October 2015). In contrast, in summer, intensified updrafts associated with

465 typhoons strengthened cloud formation, weakened solar radiation, and thus restrained local O_3 production. Longer APRTs (>

466 20 hour) under typhoon influence were far from sufficient to maintain high contributions of local emissions for O_3 pollution

467 (which decreased by ~20% for the polluted regions of the PRD in July 2016). However, due to the variations of wind fields

468 under different scenarios, the changes of local and transport contributions for O_3 led by typhoons were different in the

469 southwest part of the PRD, that is, higher contribution from emissions within the PRD and reduced transport contribution

470 occurred in the typhoon-induced scenarios in both seasons. As for the close typhoon-induced scenario, O_3 transport was further

471 strengthened, but meteorological conditions in the PRD became less favourable for both the production and accumulation of
472 O_3.
473
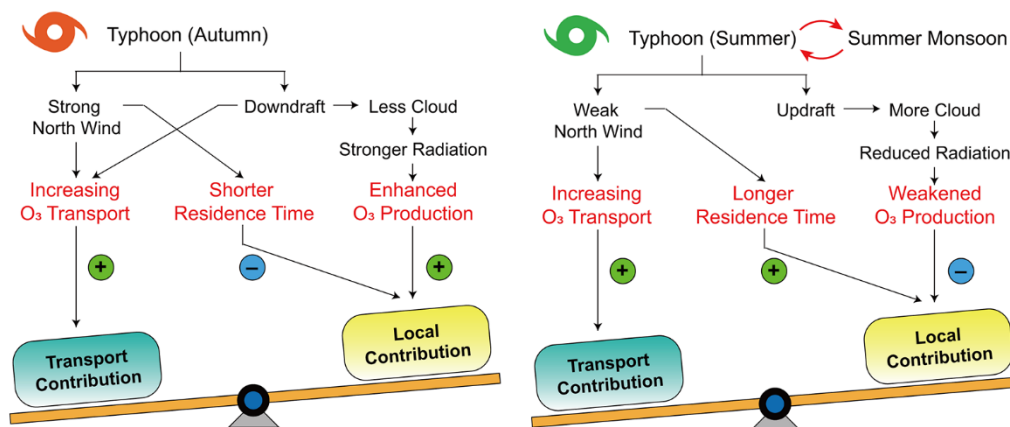
474
475 **Figure 11.** The summary of the causes of O_3 pollution in the PRD under typhoon influence in autumn and summer.

476 The East Asian monsoon, changing with seasons, has a pronounced impact on local meteorological conditions as well as the
477 characteristics of O_3 pollution in East China (He et al., 2008). The seasonal behaviour of the East Asian monsoon is likely to
478 result in the seasonally varied effect of typhoons on O_3 pollution in the PRD. In October, the summer monsoon has almost
479 finished its retraction and the winter monsoon is beginning (Ding, 1994). Thus, there are not many obstacles to the southward
480 movement of typhoon periphery and the transport of O_3 towards the PRD by the continental and coastal air masses. Large
481 downdraft-influenced areas in Central and South China occur in this scenario, and high O_3 levels and low RH in these areas
482 indicate the potentially important role of directly downward O_3 transport. In July, the summer monsoon reaches its strongest
483 (Ding, 1994). The interaction between typhoon periphery and the summer monsoon results in stagnation and enhanced updrafts
484 above the land areas of the PRD and its surroundings. Only when typhoon is close enough to the PRD is the stagnation
485 terminated and the structure of the summer monsoon cell broken. This also explains why some summertime typhoon-induced
486 O_3 episodes in the PRD can be typically divided into two periods, as stagnation leads to the accumulation of locally produced
487 O_3 in the first phase and strong northerly winds strengthen O_3 transport before the landing of typhoons (Lam et al., 2005; Li,
488 2013). It should be noted that updrafts, rather than downdrafts, prevailed on the typhoon-induced O_3 pollution days in summer.
489 High levels of O_3 did not necessarily occur in the regions dominated by downdrafts in this scenario, suggesting a less notable
490 connection between downdrafts and summertime O_3 pollution in the PRD. Further investigations are required to trace the
491 detailed process of downward O_3 transport, including the stratosphere-troposphere exchange (Stohl et al., 2003), in each
492 scenario, and quantify their contributions to near-ground O_3 pollution.
493

494 Some limitations remain in this study. We chose O_3 pollution days as individual samples, ignoring the influence of O_3 pollution

495 on the previous days. Thus, more detailed full-episode analyses are required. Moreover, owing to the small sampling size, the

496 influence of typhoons on O_3 pollution in the PRD is still not fully understood, including, for instance, the detailed connections

497 between the features of typhoons (intensity, position) and O_3 pollution. However, the comparisons of meteorological conditions,

498 O_3 processes and sources in different scenarios and seasons demonstrate the complex causes of typhoon-induced O_3 pollution

499 in the PRD — typhoons tend to enhance O_3 transport into the PRD in both seasons, but their impacts on the production and

500 accumulation of O_3 are completely different. As a result, emissions within (outside of) the PRD are likely to contribute less

501 (more) on the typhoon-induced O_3 pollution days than on the no-typhoon days. In order to effectively alleviate O_3 pollution

502 and to reduce the population exposure in the PRD, more attention should be paid to controlling anthropogenic emissions of O_3

503 precursors on a larger scale, rather than focusing on local emission, under typhoon influence. For air quality management, it

504 is suggested to comprehensively evaluate the efficiency of fractional local and non-local emission reductions to reduce O_3

505 levels in the PRD in different scenarios (Thunis et al., 2019; Thunis et al., 2020). This study also suggests that a thorough

506 evaluation of O_3 transport, production and accumulation conditions can be applied to understand the causes of regional O_3

507 pollution not only in the PRD, but also in other regions. The results will help find efficient strategies to alleviate regional O_3

508 pollution as well as to reduce its adverse effects.

509

510 *Data availability.* Data are available from the corresponding author upon request.

511

512 *Author contributions.* KQ, XW and YZ designed the study. KQ, XW, and TX did the simulation work, including the operation

513 of the WRF, SMOKE and CMAQ models. JS, HD, LZ and YZ provided observational results of field campaigns and the

514 routine monitoring datasets for the evaluation of model performance. KQ, XW, YY and YZ analysed the modelling results.

515 KQ, XW, YY and YZ wrote and revised this paper, with critical feedbacks from all other authors.

516

517 *Competing interests*. The authors declare no conflict of interest.

518

519 *Acknowledgements*. This work was supported by the National Key Research and Development Program of China (Grant No.

520 2018YFC0213204,2018YFC0213506, 2018YFC0213501) and the National Science and Technology Pillar Program of China

521 (Grant No. 2014BAC21B01).

522

523 **References**

524 Berrisford, P., Dee, D., Poli, P., Brugge, R., Fielding, K., Fuentes, M., Kallberg, P., Kobayashi, S., Uppala, S., and Simmons,
525   A.: The ERA-Interim archive Version 2.0, ERA report series, 1, 1–16, 2011.

526 Carter, W. P. L.: Development of the SAPRC-07 chemical mechanism, Atmos. Environ., 44, 5324–5335,
527   https://doi.org/10.1016/j.atmosenv.2010.01.026, 2010.

528 Chen, H., Wang, X., Shen, J., Lu, K., and Zhang, Y.: Ozone source apportionment of typical photochemical pollution
529   episodes in the Pearl River Delta in autumn, Acta Scientiarum Naturalium Universitatis Pekinensis (in Chinese), 51,
530   620–630, https://doi.org/10.13209/j.0479-8023.2015.089, 2015.

531 Chen, Q., Miao, J., and Li, W.: A comparison of mean wind field and mean meridional circulation between south-west
532   monsoon area in Southeast Asia and Pacific trade wind area in July, 1958, Acta Meteorologica Sinica (in Chinese),
533   34(1), 51–61, https://doi.org/10.11676/qxxb1964.006, 1964.

534 Chen, X., Liu, Y., Lai, A., Han, S., Fan, Q., Wang, X., Ling, Z., Huang, F., and Fan, S.: Factors dominating 3-dimensional
535   ozone distribution during high tropospheric ozone period, Environ. Pollut., 232, 55–64,
536   https://doi.org/10.1016/j.envpol.2017.09.017, 2018.

537 Chow, E. C., Li, R. C., and Zhou, W.: Influence of tropical cyclones on Hong Kong air quality, Adv. Atmos. Sci., 35(9),
538   1177–1188, https://doi.org/10.1007/s00376-018-7225-4, 2018.

539 Chow, E. C., Wen, M., Li, L., Leung, M. Y., Cheung, P. K., and Zhou, W.: Assessment of the Environmental and Societal
540   Impacts of the Category-3 Typhoon Hato, Atmosphere, 10(6), 296. https://doi.org/10.3390/atmos10060296, 2019.

541 Clappier, A., Belis, C. A., Pernigotti, D., and Thunis, P.: Source apportionment and sensitivity analysis: two methodologies
542   with two different purposes, Geosci. Model Dev., 10, 4245–4256, https://doi.org/10.5194/gmd-10-4245-2017, 2017.

543 Dee, D. P., Uppala, S. M., Simmons, A. J., Berrisford, P., Poli, P., Kobayashi, S., Andrae, U., Balmaseda, M. A., Balsamo,
544   G., Bauer, P., Bechtold, P., Beijaars, A.C.M., van de Berg, L., Bidiot, J., Bormann, N., Delsol, C., Dragani, R., Fuentes,
545   M., Geer, A.J., Haimberger, L., Healy, S.B., Hersbach, H., Hólm, E.V., Isaksen, L., Isaksen, L., Kållberg, P., Köhler,
546   M., Matricardi, M., McNally, A.P., Monge-Sanz, B.M., Morcrette, J.-J., Park, B.-K., Peubey, C., de Rosnay, P.,
547   Tavolato, Thépaut, J.-N., and Vitart, F.: The ERA−Interim reanalysis: Configuration and performance of the data
548   assimilation system, Q. J. Roy. Meteor. Soc., 137(656), 553–597, https://doi.org/10.1002/qj.828, 2011.

549 Deng, T., Wang, T., Wang, S., Zou, Y., Yin, C., Li, F., Liu, L., Wang, N., Song, L., Wu, C., and Wu, D.: Impact of typhoon
550   periphery on high ozone and high aerosol pollution in the Pearl River Delta region, Sci. Total Environ., 668, 617–630,
551   https://doi.org/10.1016/j.scitotenv.2019.02.450, 2019.

552 Ding, Y. H.: Monsoons over China, Kluwer Academic Publishers, Dordrecht/Boston/London, 1994.

553 Ding, Y., Si, D., Liu, Y., Wang, Z., Li, Y., Zhao, L., and Song, Y.: On the Characteristics, Driving Forces and Inter-decadal
554   Variability of the East Asian Summer Monsoon, Chinese Journal of Atmospheric Sciences (in Chinese), 42(3), 533–
555   558, https://doi.org/10.3878/j.issn.1006-9895.1712.17261, 2018.

556 Feng, Y., Ning, M., Lei, Y., Sun, Y., Liu, W., and Wang, J.: Defending blue sky in China: Effectiveness of the "Air
557 Pollution Prevention and Control Action Plan" on air quality improvements from 2013 to 2017, J. Environ. Manage.,
558 252, 109603, https://doi.org/10.1016/j.jenvman.2019.109603, 2019.

559 Gao, X., Deng, X., Tan, H., Wang, C., Wang, N., and Yue, D.: Characteristics and analysis on regional pollution process and
560 circulation weather types over Guangdong Province, Acta Scientiae Circumstantiae (in Chinese), 38(5), 1708–1716,
561 https://doi.org/10.13671/j.hjkxxb.2017.0473, 2018.

562 Guo, J., Miao, Y., Zhang, Y., Liu, H., Li, Z., Zhang, W., He, J., Lou, M., Yan, Y., Bian, L., and Zhai, P.: The climatology of
563 planetary boundary layer height in China derived from radiosonde and reanalysis data, Atmos. Chem. Phys., 16, 13309–
564 13319, https://doi.org/10.5194/acp-16-13309-2016, 2016.

565 He, K.: Multi-resolution Emission Inventory for China (MEIC): model framework and 1990-2010 anthropogenic emissions,
566 American Geophysical Union, Fall Meeting 2012, San Francisco, the United States of America, 3–7 December 2012,
567 A32B-05, 2012.

568 He Y. J., Uno, I., Wang, Z. F., Pochanart, P., Li, J., and Akimoto, H.: Significant impact of the East Asia monsoon on ozone
569 seasonal behavior in the boundary layer of Eastern China and the west Pacific region, Atmos. Chem. Phys., 8, 7543–
570 7555, https://doi.org/10.5194/acp-8-7543-2008, 2008.

571 Huang, J. P., Fung, J. C., Lau, A. K., and Qin, Y: Numerical simulation and process analysis of typhoon−related ozone
572 episodes in Hong Kong, J. Geophys. Res.-Atmos., 110(D5), https://doi.org/10.1029/2004JD004914, 2005.

573 Huang, Y., Yao, T., Fung, J. C., Lu, X., and Lau, A. K.: Application of air parcel residence time analysis for air pollution
574 prevention and control policy in the Pearl River Delta region, Sci. Total Environ., 658, 744–752,
575 https://doi.org/10.1016/j.scitotenv.2018.12.205, 2019.

576 Jin, Q., Yang, X. Q., Sun, X. G., and Fang, J. B.: East Asian summer monsoon circulation structure controlled by feedback
577 of condensational heating, Clim. Dynam., 41(7-8), 1885–1897, https://doi.org/10.1007/s00382-012-1620-9, 2013.

578 Jiang, F., Wang, T., Wang, T., Xie, M., and Zhao, H.: Numerical modeling of a continuous photochemical pollution episode
579 in Hong Kong using WRF–chem, Atmos. Environ., 42(38), 8717–8727,
580 https://doi.org/10.1016/j.atmosenv.2008.08.034, 2008.

581 Lam, K. S., Wang, T. J., Wu, C. L., and Li, Y. S.: Study on an ozone episode in hot season in Hong Kong and transboundary
582 air pollution over Pearl River Delta region of China, Atmos. Environ., 39(11), 1967–1977,
583 https://doi.org/10.1016/j.atmosenv.2004.11.023, 2005.

584 Lam, Y. F.: Climate change and air quality in Southeastern China: Hong Kong study, in: Climate change and air pollution,
585 edited by: Akhtar R., and Palagiano C., Springer, Cham, 181–196, https://doi.org/10.1007/978-3-319-61346-8_12,
586 2018.

587 Lam, Y. F., Cheung, H. M., and Ying, C. C.: Impact of tropical cyclone track change on regional air quality, Sci. Total
588 Environ., 610, 1347–1355, https://doi.org/10.1016/j.scitotenv.2017.08.100, 2018.

589 Li, J., Lu, K., Lv, W., Li, J., Zhong, L., Ou, Y., Chen, D., Huang, X., and Zhang, Y.: Fast increasing of surface ozone
590   concentrations in Pearl River Delta characterized by a regional air quality monitoring network during 2006–2011, J.
591   Environ. Sci., 26(1), 23–36, https://doi.org/10.1016/S1001-0742(13)60377-0, 2014.

592 Li, M., Jiang, S., Gan, Q., Chen, F., Zeng, D., Li, J., Fan, S., and Zhu, W.: Characteristics of ozone pollution and analysis of
593   typical pollution processes in summer and autumn in Huizhou, Acta Scientiarum Naturalium Universitatis Sunyatseni
594   (in Chinese), 57(5), 29, https://doi.org/10.13471/j.cnki.acta.snus.2018.05.004, 2018.

595 Li, M., Zhang, Q., Kurokawa, J.-I., Woo, J.-H., He, K., Lu, Z., Ohara, T., Song, Y., Streets, D. G., Carmichael, G. R., Cheng,
596   Y., Hong, C., Huo, H., Jiang, X., Kang, S., Liu, F., Su, H., and Zheng, B.: MIX: a mosaic Asian anthropogenic emission
597   inventory under the international collaboration framework of the MICS-Asia and HTAP, Atmos. Chem. Phys., 17, 935–
598   963, https://doi.org/10.5194/acp-17-935-2017, 2017.

599 Li, K., Jacob, D. J., Liao, H., Shen, L., Zhang, Q., and Bates, K. H.: Anthropogenic drivers of 2013–2017 trends in summer
600   surface ozone in China, P. Natl. Acad. Sci. USA, 116(2), 422–427, https://doi.org/10.1073/pnas.1812168116, 2019.

601 Li, Y.: The evolution characteristics and source analysis of the secondary pollutants in summer over Pearl River Delta, Ph.D.
602   thesis, College of Environmental Science and Engineering, Peking University, China, 160 pp., 2013.

603 Li, Y., Lau, A. K. H., Fung, J. C. H., Zheng, J.Y., Zhong, L. J., and Louie, P. K. K.: Ozone source apportionment (OSAT) to
604   differentiate local regional and super-regional source contributions in the Pearl River Delta region, China, J. Geophys.
605   Res.-Atmos., 117, D15305, http://doi.org/10.1029/2011JD017340, 2012.

606 Liou, K. N.: On the absorption, reflection and transmission of solar radiation in cloudy atmospheres, J. Atmos. Sci., 33(5),
607   798–805, https://doi.org/10.1175/1520-0469(1976)033<0798:OTARAT>2.0.CO;2, 1976.

608 Lin, X., Yuan, Z., Yang, L., Luo, H., and Li, W.: Impact of extreme meteorological events on ozone in the Pearl River Delta,
609   China, Aerosol Air Qual. Res., 19(6), 1307–1324, https://doi.org/10.4209/aaqr.2019.01.0027, 2019.

610 Liu, H., Liu, S., Xue, B., Lv, Z., Meng, Z., Yang, X., Xue, T., Yu, Q., and He, K.: Ground-level ozone pollution and its
611   health impacts in China, Atmos. Environ., 173, 223–230, https://doi.org/10.1016/j.atmosenv.2017.11.014, 2018.

612 Lu, X., Hong, J., Zhang, L., Cooper, O. R., Schultz, M. G., Xu, X., Wang, T., Gao, M., Zhao, Y., and Zhang, Y.: Severe
613   surface ozone pollution in China: A global perspective, Environ. Sci. Tech. Let., 5(8), 487–494,
614   https://doi.org/10.1021/acs.estlett.8b00366, 2018.

615 Mills, G., Sharps, K., Simpson, D., Pleijel, H., Broberg, M., Uddling, J., Jaramillo, F., Davies, W. J., Dentener, F., Van den
616   Berg, M., Agrawal, M., Agrawal, S. B., Ainsworth, E. A., Büker, P., Emberson, L., Feng, Z., Harmens, H., Hayes, F.,
617   Kobayashi, K., Paoletti, E., and Van Dingenen, R.: Ozone pollution will compromise efforts to increase global wheat
618   production, Glob. Change Biol., 24, 3560–3574, https://doi.org/10.1111/gcb.14157, 2018.

619 National Research Council: Rethinking the Ozone Problem in Urban and Regional Air Pollution, Natl. Acad. Press,
620   Washington, D. C., USA, 1991.

Park, S. K., O'Neill, M. S., Stunder, B. J., Vokonas, P. S., Sparrow, D., Koutrakis, P., and Schwartz, J.: Source location of air pollution and cardiac autonomic function: trajectory cluster analysis for exposure assessment, J. Expo. Sci. Env. Epid., 17(5), 488-497, https://doi.org/10.1038/sj.jes.7500552, 2007.

Roux, F., Clark, H., Wang, K.-Y., Rohs, S., Sauvage, B., and Nédélec, P.: The influence of typhoons on atmospheric composition deduced from IAGOS measurements over Taipei, Atmos. Chem. Phys., 20, 3945–3963, https://doi.org/10.5194/acp-20-3945-2020, 2020.

So, K. L. and Wang, T.: On the local and regional influence on ground-level ozone concentrations in Hong Kong, Environ. Pollut., 123(2), 307–317, https://doi.org/10.1016/S0269-7491(02)00370-6, 2003.

Stein, A. F., Draxler, R. R., Rolph, G. D., Stunder, B. J., Cohen, M. D., and Ngan, F.: NOAA's HYSPLIT atmospheric transport and dispersion modeling system, B. Am. Meteorol. Soc., 96(12), 2059–2077, https://doi.org/10.1175/BAMS-D-14-00110.1, 2015.

Stevenson, D. S., Dentener, F. J., Schultz, M. G., Ellingsen, K., van Noije, T. P. C., Wild, O., Zeng, G., Amann, M., therton, C. S., Bell, N., Bergmann, D. J., Bey, I., Butler, T., Cofala, J., Collins, W. J., Derwent, R. G., Doherty, R. M., Drevet, J., Eskes, H. J., Fiore, A. M., Gauss, M., Hauglustaine, D. A., Horowitz, L. W., Isaksen, I. S. A., Krol, M. C., Lamarque, J.-F., Lawrence, M. G., Montanaro, V., Müller, J.-F., Pitari, G., Prather, M. J., Pyle, J. A., Rast, S., Rodriguez, J. M., Sanderson, M. G., Savage, N. H., Shindell, D. T., Strahan, S. E., Sudo, K., and Szopa, S.: Multimodel ensemble simulations of present-day and near-future tropospheric ozone, J. Geophys. Res., 111, D08301, https://doi.org/10.1029/2005JD006338, 2006.

Stohl, A., Bonasoni, P., Cristofanelli, P., Collins, W., Feichter, J., Frank, A., Forster, C., Gerasopoulos, E., Gaggeler, H., James, P., Kentarchos, T., Kromp-Kolb, H., Kruger, B., Land, C., Meloen, J., Papayannis, A., Priller, A., Seibert, P., Sprenger, M., Roelofs, G. J., Scheel, H. E., Schnabel, C., Siegmund, P., Tobler, L., Trickl, T., Wernli, H., Wirth, V., Zanis, P., and Zerefos, C.: Stratosphere-troposphere exchange: A review, and what we have learned from STACCATO, J. Geophys. Res., 108, 8516, https://doi.org/10.1029/2002JD002490, 2003.

Thunis, P., Clappier, A., Pirovano, G.: Source apportionment to support air quality management practices, A fitness-for-purpose guide (V 3.1), EUR30263, Publications Office of the European Union, ISBN 978-92-76-19744-7, doi:10.2760/47145, JRC120764, 2020.

Thunis, P., Clappier, A., Tarrason, L., Cuvelier, C., Monteiro, A., Pisoni, E., Wesseling, J., Belis, C. A., Pirovano, G., Janssen, S., Guerreiro, C., and Peduzzi, E.: Source apportionment to support air quality planning: Strengths and weaknesses of existing approaches, Environ. Int., 130, 104825, https://doi.org/10.1016/j.envint.2019.05.019, 2019.

Wang, H., Wang, W., Huang, X., and Ding A.: Impacts of stratosphere-to-troposphere-transport on summertime surface ozone over eastern China, Sci. Bull., 65, 276–279, https://doi.org/10.1016/j.scib.2019.11.017, 2020.

Wang, N., Guo, H., Jiang, F., Ling, Z. H., and Wang, T.: Simulation of ozone formation at different elevations in mountainous area of Hong Kong using WRF-CMAQ model, Sci. Total Environ., 505, 939–951, https://doi.org/10.1016/j.scitotenv.2014.10.070, 2015.

655 Wang, T. and Kwok, J. Y: Measurement and analysis of a multiday photochemical smog episode in the Pearl River Delta of
656   China, J. Appl. Meteorol., 42(3), 404–416, https://doi.org/10.1175/1520-0450(2003)042<0404:MAAOAM>2.0.CO;2,
657   2003.

658 Wang, T., Lam, K. S., Lee, A. S., Pang, S. W., and Tsui, W. S.: Meteorological and chemical characteristics of the
659   photochemical ozone episodes observed at Cape D'Aguilar in Hong Kong, J. Appl. Meteorol., 37(10), 1167–1178,
660   https://doi.org/10.1175/1520-0450(1998)037<1167:MACCOT>2.0.CO;2, 1998.

661 Wang, T., Wu, Y. Y., Cheung, T. F., and Lam, K. S.: A study of surface ozone and the relation to complex wind flow in
662   Hong Kong, Atmos. Environ., 35(18), 3203–3215, https://doi.org/10.1016/S1352-2310(00)00558-6, 2001.

663 Wang, T., Xue, L., Brimblecombe, P., Lam, Y. F., Li, L., and Zhang, L.: Ozone pollution in China: A review of
664   concentrations, meteorological influences, chemical precursors, and effects, Sci. Total Environ., 575, 1582–1596,
665   https://doi.org/10.1016/j.scitotenv.2016.10.081, 2017.

666 Wang, X., Zhang, Y., Hu, Y., Zhou, W., Lu, K., Zhong, L., Zeng, L., Shao, M., Hu, M., and Russell, A. G.: Process analysis
667   and sensitivity study of regional ozone formation over the Pearl River Delta, China, during the PRIDE-PRD2004
668   campaign using the Community Multiscale Air Quality modeling system, Atmos. Chem. Phys., 10, 4423–4437,
669   https://doi.org/10.5194/acp-10-4423-2010, 2010.

670 Wei, X., Lam, K. S., Cao, C., Li, H., and He, J.: Dynamics of the typhoon Haitang related high ozone episode over Hong
671   Kong, Adv. Meteorol., 2016, https://doi.org/10.1155/2016/6089154, 2016.

672 Yang, J. X., Lau, A. K. H., Fung, J. C. H., Zhou, W., and Wenig, M.: An air pollution episode and its formation mechanism
673   during the tropical cyclone Nuri's landfall in a coastal city of south China, Atmos. Environ., 54, 746–753,
674   https://doi.org/10.1016/j.atmosenv.2011.12.023, 2012.

675 Ying, M., Zhang, W., Yu, H., Lu, X., Feng, J., Fan, Y., Zhu, Y., and Chen, D.: An overview of the China Meteorological
676   Administration tropical cyclone database, J. Atmos. Ocean Tech., 31(2), 287–301, https://doi.org/10.1175/JTECH-D-
677   12-00119.1, 2014.

678 Yue, H., Gu, T., Wang, C., Wu, D., Deng, X., Huang, J., and Wang, Y.: Influence of typhoon Nida process on ozone
679   concentration in Guangzhou, Acta Scientiae Circumstantiae (in Chinese), 38(12), 4565–4572,
680   https://doi.org/10.13671/j.hjkxxb.2018.0319, 2018.

681 Zhang, X., Liu, Y., Deng, X., Chen, P., Feng, Y., and Fan, Q.: Analysis of summertime typical pollution in Pearl River Delta
682   region——numerical simulation of meteorological field, Meteorological and Environmental Research, 59(4), 9–18,
683   2014.

684 Zhao, W., Gao, B., Liu, M., Lu, Q., Ma, S., Sun, S., Sun, J. Chen, L., and Fan, S.: Impact of meteorological factors on the
685   ozone pollution in Hong Kong, Huan jing ke xue= Huanjing kexue (in Chinese), 40(1), 55–66,
686   https://doi.org/10.13227/j.hjkx.201803151, 2019.

687 Zheng, J., Zhang, L., Che, W., Zheng, Z., and Yin, S.: A highly resolved temporal and spatial air pollutant emission

688   inventory for the Pearl River Delta region, China and its uncertainty assessment, Atmos. Environ., 43(32), 5112–5122,

689   https://doi.org/10.1016/j.atmosenv.2009.04.060, 2009.

690 Zheng, J., Zhong, L., Wang, T., Louie, P. K. K., and Li, Z.: Ground-level ozone in the Pearl River Delta region: Analysis of

691   data from a recently estabilished regional air quality monitoring network, Atmos. Environ., 44(6), 814–823,

692   https://doi.org/10.1016/j.atmosenv.2009.11.032, 2010.